Calculation of momentum distributions in paramagnetic chromium: Compton scattering and positron annihilation

1992 J. Phys.: Condens. Matter 4 8975

(http://iopscience.iop.org/0953-8984/4/46/005)

J. Phys.: Condens. Matter 4 (1992) 8975–8988. Printed in the UK

Calculation of momentum distributions in paramagnetic chromium: Compton scattering and positron annihilation

V Sundararajan†, D G Kanhere† and R M Singru‡

† Department of Physics, University of Poona, Pune, 411 007, India
‡ Department of Physics, Indian Institute of Technology, Kanpur, 208 016, India

Received 14 January 1992, in final form 28 May 1992

Abstract. A detailed calculation of the momentum distributions in paramagnetic (BCC) chromium is carried out using the linear combination of Gaussian orbitals (LCGO) method. Using the same electron wavefunctions, theoretical results are obtained for Compton scattering and positron annihilation, and are presented in the form of electron momentum distributions $\rho(\boldsymbol{p})$, reciprocal form factors $B(z)$, two-photon momentum distributions $\rho^{2\gamma}(\boldsymbol{p})$, one-dimensional angular correlation of positron annihilation radiation, Lock–Crisp–West distributions, etc. These results are analysed in terms of the Fermi surface topology of paramagnetic Cr. It is observed that, within the independent-particle model, the LCGO theory shows close agreement with other theories and satisfactory agreement with experiment. In particular, the present results for $\rho^{2\gamma}(p)$ are compared with those reconstructed by Kubota *et al* from their two-dimensional angular correlation of positron annihilation radiation measurements. Observed differences are ascribed to the effects of e^+–e^- many-body correlations and the reconstruction procedure.

1. Introduction

Among the 3d transition metals, the band structure and Fermi surface of paramagnetic (BCC) chromium (Cr) has invoked special research interest for some important reasons. First, Cr undergoes a phase transition from the antiferromagnetic to the paramagnetic phase at 311.5 K, and the antiferromagnetic phase further shows a spin-flip transition at 118 K. Such a magnetic ordering in Cr has been explained [1] in terms of a spin-density wave whose wavevector may be closely related to the topology of the Fermi surface of Cr in the paramagnetic phase above 311.5 K. Secondly, the band structure and Fermi surface of the VIB group of metals, paramagnetic Cr, Mo and W, show striking similarities [2] and hence are of special interest. Thirdly, Cr forms an interesting alloy system with its neighbouring element V, and knowledge of the Fermi surface of Cr is useful to understand these alloys. All this calls for a careful theoretical and experimental study of the band structure and Fermi surface of paramagnetic Cr. Experimentally, however, the conventional Fermiology methods (e.g. de Haas–van Alphen effect) require the measurements to be carried out at very low temperatures, thus making it impossible to study Cr in its paramagnetic (BCC) phase. However, the experimental techniques of Compton scattering [3, 4] and positron annihilation [5, 6], which measure the Fermi surface through the momentum distributions, do not suffer from this limitation. In view of this, the paramagnetic phase of Cr has been studied by measuring directional Compton profiles [7–9] and one-dimensional (1D)

0953-8984/92/468975+14$07.50

or two-dimensional (2D) angular correlation of positron annihilation radiation (ACAR) [10–15]. Usually the electron momentum distributions $\rho(\boldsymbol{p})$ involved in Compton scattering and the two-photon momentum distributions $\rho^{2\gamma}(\boldsymbol{p})$ involved in positron annihilation are theoretically calculated within the independent-particle model (IPM) using an established band-structure method [4, 6]. For a more complete description, it is necessary to include e^-–e^- correlations [4] in $\rho(\boldsymbol{p})$ and positron wavefunction as well as e^+–e^- many-body correlations [6] in $\rho^{2\gamma}(\boldsymbol{p})$. It has been shown [16, 17] that the effect of e^-–e^- correlations on $\rho(\boldsymbol{p})$ is to raise some electrons from levels just below the Fermi level ($p = p_F$) to those above it. This effect reduces the height of the discontinuity (i.e. step function) that marks the Fermi surface without shifting its position from $p = p_F$. When a positron enters a metal it probes momentum distributions, which are affected by the positron wavefunction and e^+–e^- many-body correlations. As a result the shape of $\rho^{2\gamma}(\boldsymbol{p})$ is different from that of $\rho(\boldsymbol{p})$ although both distributions display discontinuities at $p = p_F$ [18]. Valuable information about the Fermi surface of a transition metal can thus be obtained by a complementary study of $\rho(\boldsymbol{p})$ and $\rho^{2\gamma}(\boldsymbol{p})$. For a systematic understanding of the above effects it is useful to calculate $\rho(\boldsymbol{p})$ and $\rho^{2\gamma}(\boldsymbol{p})$ using the same set of electron wavefunctions and the same band-structure method.

Theoretical Compton profiles for paramagnetic Cr have been calculated by (i) Wakoh *et al* [19] using the augmented plane-wave (APW) method, (ii) Rath *et al* [20] using the linear combination of atomic orbitals (LCAO) method and (iii) Laurent *et al* [21] using the linear combination of Gaussian orbitals (LCGO) method and the Kohn–Sham–Gaspar exchange potential. Recently Cardwell and Cooper [22] have shown that better treatment of exchange and correlation effects in the LCGO theory is important for an accurate description of the Compton profiles of paramagnetic Cr. Cardwell *et al* [9] and Wakoh and Matsumoto [23] have carried out a more comprehensive calculation of the Compton profiles in paramagnetic Cr incorporating the electron correlation effects. The calculation of $\rho^{2\gamma}(\boldsymbol{p})$ in paramagnetic Cr has been carried out using the APW [10, 24, 25], Hubbard–Mijnarends [26–28] and linear muffin-tin orbitals (LMTO) [13, 14] methods.

Keeping all this work in mind, we have carried out a more detailed calculation of $\rho(\boldsymbol{p})$ and $\rho^{2\gamma}(\boldsymbol{p})$ in paramagnetic Cr by incorporating two improvements in the previously reported LCGO method [21]. First, the treatment of exchange and correlation potential has been improved. Secondly, the LCGO method has been extended [29] so that $\rho^{2\gamma}(\boldsymbol{p})$ and ACAR distributions, in addition to $\rho(\boldsymbol{p})$ and Compton profiles, can be calculated using the same set of electron wavefunctions. The results of the present calculations have been analysed in terms of the Fermi surface of paramagnetic Cr and compared with the experimentally measured Compton profiles and ACAR data for paramagnetic Cr. In particular, the theoretical $\rho^{2\gamma}(\boldsymbol{p})$ curves calculated by us are compared with experimental $\rho^{2\gamma}(\boldsymbol{p})$ reconstructed by Kubota *et al* [15] from 2D ACAR data sets.

2. Calculational procedure

The all-electron self-consistent LCGO method used by us to calculate $\rho(\boldsymbol{p})$ and $\rho^{2\gamma}(\boldsymbol{p})$ has been described elsewhere [29–31], and it carries certain advantages like its self-consistent character and the absence of any shape-dependent approximations. Another advantage of this method relevant for the calculation of these momentum distributions is the Gaussian nature of the basis functions, which allows one to compute $\rho(\boldsymbol{p})$ and $\rho^{2\gamma}(\boldsymbol{p})$ up to a desired high value of momentum ($\boldsymbol{p}$) analytically and

accurately. This feature assures greater accuracy because the Compton profiles (or ACAR curves) are obtained from $\rho(p)$ or $\rho^{2\gamma}(p)$ by a numerical integration in the p-space. A basic doubt might be expressed about the validity of the Kohn–Sham single-particle orbitals for the calculation of these momentum distributions, particularly from the point of view of incorporating many-body effects. However, previous calculations of the Compton profiles of V [32, 33], Cr [21], Fe [20, 34], Ni [35, 36], Nb [37], Pd [38] and Ag [39] and ACAR curves of V [33], Fe [34], Ni [29] and Cu [29, 40] performed with the self-consistent LCGO method have shown that, within the independent-particle model (IPM), these results show good agreement with other band theories (e.g. APW) and satisfactory agreement with experiment. The residual many-body effects that are not taken into account in the present LCGO method (within IPM) can be added later as corrections. Although this might appear as an *ad hoc* solution to the many-body problem, similar procedures have been applied (see discussion in the next section) for the LMTO [13, 14, 41] and APW [25] methods to bring theory closer to experiment. Such an *ad hoc* procedure is made necessary by the difficulties involved in treating the many-body effects using an *ab initio* approach.

Another effect that can cause some inaccuracy in the present LCGO method (and in some other IPM methods) is the neglect of the non-local nature of the exchange–correlation potential. Our calculations for Cu using the non-local potential in the LCGO method [42] have indicated that non-locality causes less than 4% change in the momentum distributions while the bandwidths change by 5–10 mRyd. The effect on the Fermi surface topology was observed to be minor. Barbiellini and Jarlborg [43] have used non-local potentials in their self-consistent calculations of the band structure of V, Cu, Nb and Pd using the LMTO method, and have observed that the non-locality in exchange and correlation causes minor changes in the properties of the Fermi surface of these metals. For example, it was found that the non-locality slightly reduces the size of third-band distorted ellipsoidal hole surfaces centred at N in V. In other studies [13, 14] the effect of non-locality has been simulated for Fe by treating the centre of gravity E_ν of d bands (calculated within the local-density approximation) as a parameter. The values of E_ν were displaced by few mRyd so that a better agreement was obtained with the experimental results for the Fermi surface. Such a parametrization also caused minor changes in the momentum distributions. In view of the fact that there is no experimental determination of the Fermi surface of paramagnetic Cr, we could not attempt a similar simulation of non-local effects in the present work.

The present calculations used the Gaussian basis set consisting of thirteen s, ten p, five d and one f functions with the value of lattice constant $a = 5.4419$ au. The previous LCGO calculation of the Compton profile (CP) by Laurent *et al* [21] used the Kohn–Sham–Gaspar exchange potential, while the present work used the exchange–correlation potential of von Barth and Hedin [44] as modified by Rajagopal *et al* [45]. The positron wavefunction (with Γ_1 symmetry) was calculated within the framework of LCGO theory using seven s Gaussian orbitals, and by reversing the sign of the electron potential and removing the exchange part. The distributions $\rho(p)$ contributed by the band electrons were calculated up to $p = 10.0$ au by using a total of 2123 reciprocal lattice vectors. The distributions, so calculated, resulted in a value of 5.98 band electrons, thus indicating the high accuracy involved. The distributions, $\rho^{2\gamma}(p$ were computed up to $p = 4.0$ au using a total of 135 reciprocal lattice vectors. It is pointed out that these calculations were carried out in the IPM, and no corrections were made for the e^-–e^- or for e^+–e^- correlations in the first stage.

3. Results and discussion

3.1. Band structure and Fermi surface

The electronic band structure and Fermi surface of paramagnetic Cr obtained by us are similar to those reported by Laurent *et al* [21]. The density of states $N(E = E_F)$ at the Fermi energy is found to be 9.67 states/ atom Ryd, which compares well with other theoretical values of 9.41 states/ atom Ryd [21] and 9.51 states/ atom Ryd [46]. The Fermi surface of paramagnetic Cr is shown schematically in figure 1 and it displays the following familiar features: (i) the fourth band (the 4s Γ_1 level being numbered as the first band) electron jack (e_4) centred at the point Γ; (ii) the third-band octahedral hole pockets (h_3) centred at the point H; (iii) the third-band ellipsoidal hole pockets (h_3) centred at the point N; and (iv) the fifth-band thin electron lenses (e_5) lying along the symmetry axes Δ (joining Γ to H). This topology of the Fermi surface will be useful later during our discussion of the structures observed in our results for $\rho(p)$ and $\rho^{2\gamma}(p)$.

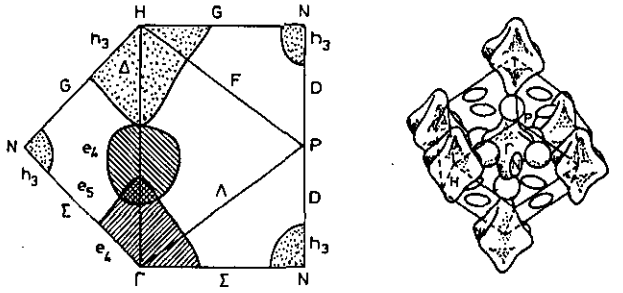

Figure 1. Fermi surface of paramagnetic Cr.

3.2. Distributions $\rho(p)$ and Compton profiles

To test the quality of the electron wavefunctions obtained by us for paramagnetic Cr, we first calculated $\rho(p)$ and directional Compton profiles. The results for $\rho(p)$ contributed by the band electrons of paramagnetic Cr along the three directions ⟨100⟩, ⟨110⟩ and ⟨111⟩ are shown in figure 2. Comments on the shape and structure in these distributions will be made later when we shall discuss the results for $\rho^{2\gamma}(p)$. At this stage we only point out that the plots shown in figure 2 can be useful in future for comparing theory with experimental $\rho(p)$ reconstructed from a set of directional Compton profiles measured with high resolution. Such a reconstruction of $\rho(p)$ in Fe has already been attempted using a set of 14 directional Compton profiles [47] .

A comparison of the present results for the weighted areas under the pure s-, p- and d-wave contributions to $\rho(p)$ and $\rho^{2\gamma}(p)$ along the ⟨100⟩, ⟨110⟩ and ⟨111⟩ directions in paramagnetic Cr is shown in table 1. It is observed from these results that the angular momentum dependence of these momentum distributions is highly anisotropic with the percentage of d contributions being highest for $\rho(p)$ along the ⟨111⟩ direction. We feel that this behaviour can give rise to anisotropy in the $e^- - e^-$ correlation effects observed in the Compton profile data [9].

Using the results for $\rho(p)$ we computed the Compton profiles along the ⟨100⟩, ⟨110⟩ and ⟨111⟩ directions. These directional Compton profiles contributed by the

Table 1. The ratio of the weighted areas of pure s, p and d contributions [a] to the total momentum distributions in paramagnetic Cr.

Direction	State					
	s		p		d	
	$\rho(p)$	$\rho^{2\gamma}(p)$	$\rho(p)$	$\rho^{2\gamma}(p)$	$\rho(p)$	$\rho^{2\gamma}(p)$
⟨100⟩	0.103	0.111	0.115	0.115	0.741	0.600
⟨110⟩	0.100	0.196	0.074	0.135	0.791	0.580
⟨111⟩	0.043	0.090	0.058	0.093	0.645	0.450

[a] The sum of s, p and d contributions along any direction does not add up to 1.000 because the hybridized part is not taken into account.

band electrons showed a close agreement with the previous calculations using the LCGO method [21]. Total (i.e. core + band) Compton profiles were obtained by adding the contribution of core electrons (reported by Biggs *et al* [48]) to that of band electrons. The total Compton profiles so obtained for the ⟨100⟩, ⟨110⟩ and ⟨111⟩ directions were compared with the theoretical APW and LCAO results (as reported by Cardwell *et al* [9]) and experimental results [9] after proper convolution with the detector resolution function (Gaussian having FWHM = 0.40 au). Such a comparison once again showed a close agreement between the present results and the other (i.e. APW and LCAO) theories. However, a comparison of the present results for the directional Compton profile $J(p_z)$ and the difference curves $\Delta J(p_z) = (J_{110} - J_{100})$, etc, with measured $J(p_z)$ and $\Delta J(p_z)$ curves [9] showed discrepancies observed previously when the APW and LCAO theories were compared with experiment. Thus the present theoretical $J(p_z)$ curves showed similar shapes to the measured $J(p_z)$ curves but the theory seemed to overestimate the Compton profile in the low-momentum region ($p_z < 1.0$ au). In the case of the difference curves $\Delta J(p_z)$, satisfactory agreement was obtained with the experiment for the ([110] – [100]) directions for the general shape and pitch of the oscillatory curves, with the theory showing larger amplitudes. The agreement for the ([111] – [100]) and ([111] – [110]) directions was not so good. Results of a similar comparison have been presented by Cardwell *et al* [9], and hence we have not shown them here. Such discrepancies between theory and experiment have been observed in other 3d metals, and they have been attributed to the effects of e^-–e^- correlation. Cardwell *et al* [9] and Wakoh and Matsumoto [23] have successfully shown how to calculate the anisotropic e^-–e^- correlation effects for the directional Compton profiles of Cr. Since the present theory is based on the local-density approximation, the e^-–e^- correlation effects have to be included separately. We attempted to include these effects by using the tables of correlation correction terms given by Cardwell *et al* [9], although their APW density-of-states function might be different from the present LCGO theory. We observed that such a treatment brought the present theory in closer agreement with experiment, although small residual disagreement still remained. A conclusion reached by us after making all these comparisons is that within the IPM the quality of the present LCGO electron wavefunctions is as good as that obtained from the APW and previous LCAO theories, and that they provide a good basis to describe the momentum distributions in paramagnetic Cr.

In order to analyse the theoretical Compton profiles further, we have computed their Fourier transform $B(z)$, also known as the reciprocal form factor or autocorrelation function in the literature [4, 5]. The directional $B(z)$ functions obtained by

us along the [100], [110] and [111] directions are shown in figure 3, and they show an anisotropy in position space arising out of the charge asphericity (of the d states in particular) in paramagnetic Cr. We could not construct the experimental $B(z)$ curves because the measured Compton profiles were available for a small number of points [9]. It is well known [49, 50] that, in solids having fully occupied Brillouin zones (BZ), $B(z) = 0$ whenever $z = z_i$, the lattice vector. This condition is, however, not fulfilled in metals and the zero crossings of $B(z)$ do not occur at $z = z_i$. In paramagnetic Cr the values of z_i along the [100], [110] and [111] directions occur at 5.44, 7.70 and 4.71 au respectively. The theoretical $B(z)$ functions (figure 3) consist of pronounced minima along the [100] and [110] directions and a pronounced shoulder-like structure along the [111] direction. The zeros of $B(z)$ are observed (figure 2) at $z = 3.1$, $z = 4.85$ and $z = 6.8$ au along the [100] direction and at $z = 7.5$ and 11.0 au along the [110] direction. This behaviour does not indicate any systematic pattern, and it is difficult to explain it in simple terms. It has been pointed out that there is a preferential (72%) occupancy of t_{2g} orbitals along the nearest-neighbour [111] directions in paramagnetic Cr [9]. We feel that this fact might be related to the shoulder exhibited by the $B(z)$ curve in the range $z = 4$–8 au along the [111] direction.

3.3. Distributions $\rho^{2\gamma}(p)$ and ACAR curves

The results for $\rho^{2\gamma}(p)$ due to the band electrons of paramagnetic Cr calculated by us are presented in figures 2, 4 and 5 in different ways. While the directional behaviour of $\rho^{2\gamma}(p)$ along the important symmetry directions $\langle 100 \rangle$, $\langle 110 \rangle$ and $\langle 111 \rangle$ is brought out in figure 2, the surfaces $\rho^{2\gamma}(p_x, p_y, p_z = 0)$ in the (001) and (110) planes passing through the Γ point (centre of the BZ) are shown in figures 4(*a*) and (*b*) respectively. The contours of the $\rho^{2\gamma}(p)$ surfaces in the (001), (110) and $(1\bar{1}2)$ planes passing through the Γ point are shown in figures 5(*a*), (*b*) and (*c*) respectively. As expected, the general shapes of $\rho(p)$ and $\rho^{2\gamma}(p)$ and the structures appearing in them (figure 2) are similar, the differences being due to the effects of positron wavefunction. While the general shapes of these momentum distributions are determined by the electron (and positron) wavefunctions, the characteristic structures observed in figure 2 arise out of the topology of the Fermi surface (figure 1). Thus the discontinuities occurring in the $\rho(p)$ and $\rho^{2\gamma}(p)$ curves (figure 2) on either side of the N point ($p = 0.82$ au) along the $\langle 110 \rangle$ direction and H′ point ($p = 2.0$ au) along the $\langle 111 \rangle$ direction are due to the N-centred ellipsoidal hole pocket (h_3) and H-centred octahedral hole pocket (h_3) (shown in figure 1) respectively. The Umklapp image of the N-centred ellipsoidal hole pocket is seen in the high-momentum region ($p > 2.25$ au) along the $\langle 110 \rangle$ direction.

The surfaces of $\rho^{2\gamma}(p)$ presented in figure 4 show close similarity with those calculated by the Hubbard–Mijnarends method [28] and they bring out the topology of the Fermi surface of paramagnetic Cr in greater detail. Thus the N-centred ellipsoidal hole pocket (h_3) is observed in the (100) plane (figure 4(*a*)) in the form of hollow craters situated at $p_x = p_y = \pm(2\pi/a)/\sqrt{2}$. Similarly tower-like structures are observed in the (100) plane (figure 4(*a*)) around $p_x = \pm 1.16$ au, $p_y = \pm 1.16$ au, and they are attributed to the fourth-band electron jack (e_4) (figure 1). It is pointed out that this sheet, e_4, of the Fermi surface is prevented from contributing to $\rho(p)$ or $\rho^{2\gamma}(p)$ inside the first BZ because of the symmetry selection rule [51]. The effect of the N-centred ellipsoidal hole pocket (h_3) is also seen in the (110) plane (figure 4(*b*)) in the form of hollow craters. Also seen in figure 4(*b*) are the effects of H-centred

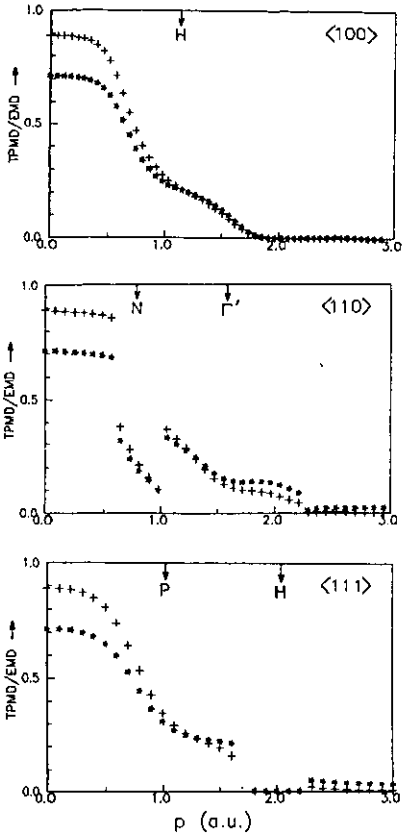

Figure 2. Theoretical (LCGO) $\rho(p)$ (*) and $\rho^{2\gamma}(p)$ (+) contributed by the band electrons of paramagnetic Cr along the ⟨100⟩, ⟨110⟩ and ⟨111⟩ directions.

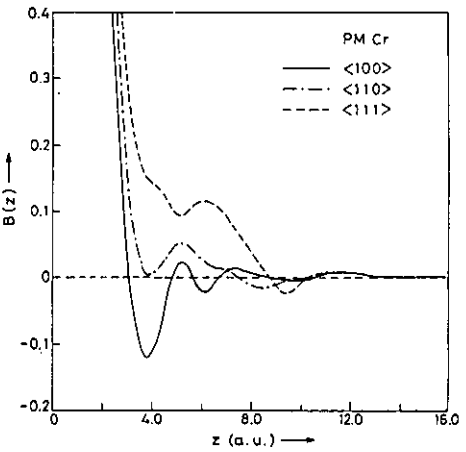

Figure 3. Theoretical (LCGO) $B(z)$ functions in paramagnetic Cr along the ⟨100⟩, ⟨110⟩ and ⟨111⟩ directions. The theoretical Compton profiles were convoluted with a Gaussian of FWHM = 0.40 au before taking the Fourier transform.

octahedral hole pockets (h_3) at $p_x = \pm(2\pi/a)$, $p_y = 0$ and the effects of the Γ-centred electron jack (e_4) around Γ, i.e. $p_x = 0, p_y = \sqrt{2}(2\pi/a)$. A better visual presentation of these structures is available in the contour plots shown in figure 5. Thus the effect of the N-centred ellipsoidal hole pocket (h_3) in the $(1\bar{1}2)$ plane shows up effectively in figure 5(*c*) in the form of two pockets around the point N and four pockets lying on the remaining faces (lines joining P and F points). The difference in the shapes and orientation of these pockets (figure 5(*c*)) provide a valuable clue to the ellipsoidal shape of these Fermi surface sheets (e.g. the dimensions of this hole pocket along NH, NΓ and NP are approximately in the ratio 1:1.68:1.75).

In order to compare the theoretical results (figures 2, 4 and 5) with experiment we have used the results obtained by Kubota *et al* [15], who measured the 2D ACAR surfaces $N(p_y, p_z)$ for ten projections between the [010] and [110] directions of a single crystal of Cr at 323 K (i.e. the paramagnetic phase) with an experimental resolution of about 0.2 au. These workers have reconstructed $\rho^{2\gamma}(p)$ from their measured data sets $N(p_y, p_z)$, and have presented their results [15] in a form similar

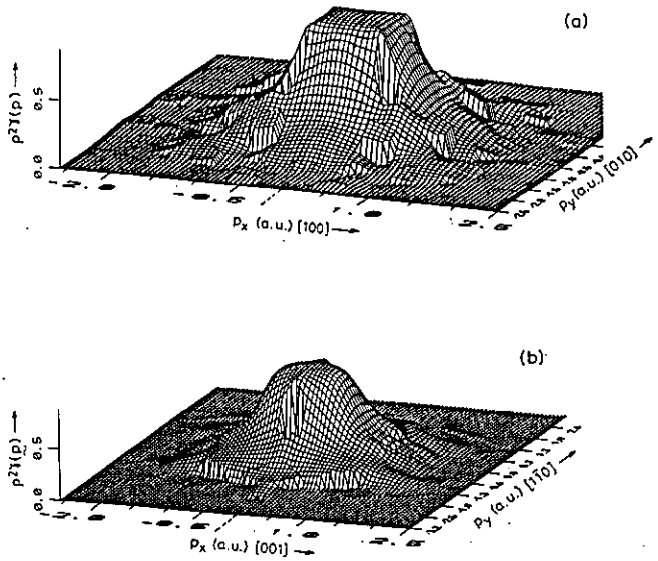

Figure 4. Plot of the surface $\rho^{2\gamma}(p_x, p_y, p_z = 0)$ passing through the Γ point in (*a*) the (001) plane and (*b*) the (110) plane of paramagnetic Cr (band electrons only).

to figures 2, 3(*a*) and 4(*a*) shown here. We have presented their results for the reconstructed $\rho^{2\gamma}(p)$ along the [100], [110] and [111] directions in figure 6. When compared to the present results (figure 2), it is observed that the general shape of the two momentum distributions along the [100] direction is very similar in the region $p > 0.35$ au (or 2.5 mrad) with the concavity in the range $p = 0.8$–1.3 au arising out of the third-band octahedral hole pocket (h_3) centred at the point H. Kubota *et al* [15] have reported a prominent peak in $\rho^{2\gamma}(p)$ around $p = 0$ (figure 6) and have ascribed it to the fourth-band electron jack (e_4) centred at the point Γ. However, this band, emanating from $\Gamma_{25'}$, does not possess the correct symmetry to contribute to $\rho^{2\gamma}(p)$ in the first BZ [51] and thus the present theoretical curves for $\rho^{2\gamma}(p)$ show a rather flat behaviour from $p = 0.0$ to $p = 0.35$ au. We feel that the peak observed by Kubota *et al* [15] in their reconstructed two-photon momentum distribution (TPMD) for $0 < p < 0.3$ au might be an effect of propagation of correlated noise [52, 53] present in their reconstruction scheme. It may be pointed out that we have avoided superimposing theoretical curves (figure 2) on the experimental curves (figure 6) because, in addition to the normalization problem, our IPM theory did not contain a contribution from core electrons (although it is rather small) or e^+–e^- many-body correlations. Our main aim in comparing theory with experiment is to look for the structures that can be related to the Fermi surface (FS) topology for a better understanding of their origin.

It is further observed that, compared to experiment (figure 6), theoretical $\rho^{2\gamma}(p)$ curves display much sharper structures along the [110] and [111] directions (figure 2). The same conclusion is drawn when the contour plot in figure 5(a) is compared with a similar plot reported by Kubota *et al* [15]. Possible explanations for these differences could be: (i) theory overestimating the dimensions of the hole pockets centred at N and H because non-local effects have been neglected and/or (ii) the e^+–e^- many-body correlations and the effects of the instrumental resolution function (FWHM = 0.2 au) as well as the reconstruction scheme smoothing the sharp discontinuities. A similar observation was made in the case of V when theoretical $\rho^{2\gamma}(p)$ was compared with that reconstructed from experimental 2D ACAR data sets [53]. Perhaps

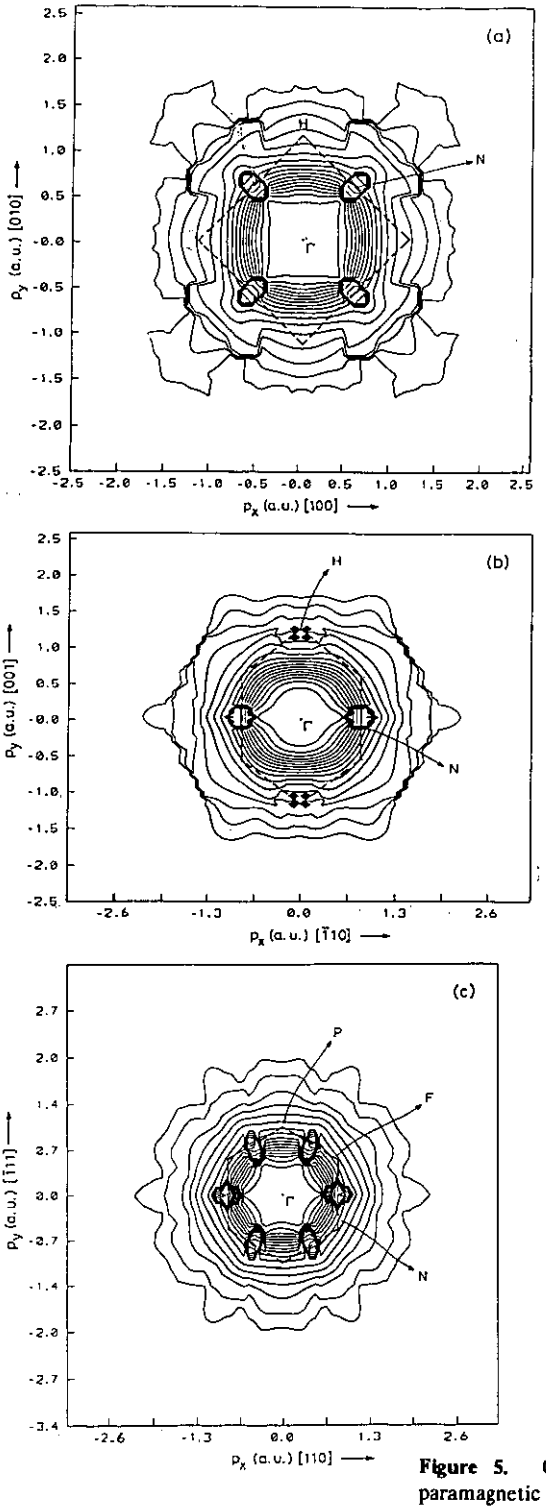

Figure 5. Contour plots of $\rho^{2\gamma}(\boldsymbol{p})$ in paramagnetic Cr (band electrons only) in (*a*) the (001) plane, (*b*) the (110) plane and (*c*) the (1$\bar{1}$2) plane passing through the Γ point.

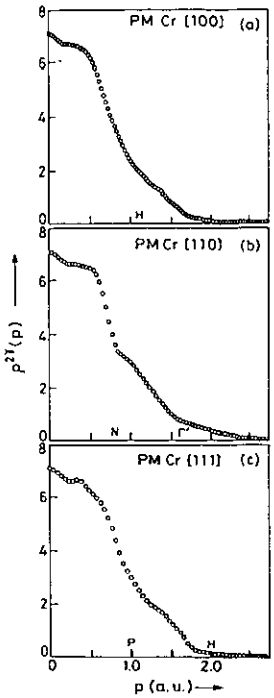

Figure 6. Experimental $\rho^{2\gamma}(p)$ in paramagnetic Cr reconstructed by Kubota *et al* [15] from their 2D ACAR data along (*a*) the [100], (*b*) the [110] and (*c*) the [111] directions.

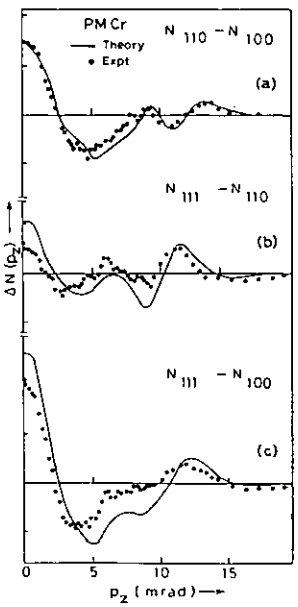

Figure 7. Difference 1D ACAR curves $\Delta N(p_z)$ in paramagnetic Cr for the ([110] – [100]), ([111] – [110]) and ([111] – [100]) directions. The full curves denote the present theory while the full circles represent experimental data [10]. The momentum scale is in mrad (milliradians) with 1 mrad $= mc \times 10^{-3} = 0.137$ au.

a reconstruction of $\rho^{2\gamma}(p)$ in other planes not passing through the Γ points (see figures 2–7 in [28]) can help to throw further light on some of these aspects.

To compare the present theory further with experiment, we have computed the 1D ACAR curves $N(p_z)$ from $\rho^{2\gamma}(p)$ and have plotted the difference curves $\Delta N(p_z) = (N_{110} - N_{100})$, etc, in figure 7. Also shown in figure 7 are the experimental $\Delta N(p_z)$ curves measured by Shiotani *et al* [10]. It is observed that there is good agreement between experiment and theory for the ([110] – [100]) directions (figure 7) even though the theory is not corrected for the e^+–e^- many-body correlations. The agreement between experiment and theory for the ([111] – [110]) and ([111] – [100]) directions is satisfactory, with theory showing similar trends but overestimating the ΔN values. Similar discrepancies were observed when the experimental data were compared with the APW theory [10] and they have been attributed to the effects of strongly d-like bands. It may be pointed out that even ΔJ, the difference Compton profile curves, associated with the [111] direction showed large discrepancies between experiment and theory [9], which were ascribed to the anistropic e^-–e^- correlations. Similarly, it has been shown that in paramagnetic Cr the e^+–e^- many-body correlation effects depends on the l value (s or p or d) of the state [13, 14] and that the t_{2g} orbitals have large (72%) occupation along [111], the nearest-neighbour directions [9]. The observed differences between the present theory and experiment for ΔN

involving ([111] – [110]) and ([111] – [100]) directions (figure 7) can, therefore, be ascribed to the effect of e^+–e^- many-body correlations.

At this stage a more detailed discussion of the e^+–e^- many-body correlation effects in paramagnetic Cr is in order. In the case of alkali metals it is usual to include these effects by multiplying $\rho^{2\gamma}(p)$, calculated in the IPM, by an isotropic enhancement factor $\epsilon(p)$. Kahana [54] proposed that for a positron in a free-electron gas one can write

$$\epsilon(p) = a + b(p/p_F)^2 + c(p/p_F)^4 \tag{1}$$

where the values of the constants a, b and c depend on the electron density and p_F ($p < p_F$) is the free-electron Fermi momentum. Although (1) has found widespread applications in the case of simple metals, its validity for non-simple metals is questionable. In particular, a different kind of enhancement is required for transition metals because of the presence of conduction bands and d bands and their hybridization. One solution to this problem was the energy-dependent 'Kahana-like' enhancement factor [55, 56]:

$$\epsilon'(E) = a + b(E/E_F) + c(E/E_F)^2 \tag{2}$$

where the energies E and Fermi energy E_F were counted from the bottom of the conduction band. Application of (2) to the 2D ACAR for Cu led to excellent agreement between theory and experiment after the core-electron contribution to theoretical $\rho^{2\gamma}(p)$ was reduced by a factor of five. In the case of other transition metals the energy-dependent formula (2) was modified [13, 14, 41] by introducing l-dependent coefficients to obtain

$$\epsilon_l(\gamma) = a_l + b_l\gamma + c_l\gamma^2 + d_l\gamma^3 \tag{3}$$

where $l = 0, 1, 2, 3$ for s, p, d and f states respectively, a_l, b_l, c_l and d_l are adjustable parameters and $\gamma = (E - E_{min})/(E_F - E_{min})$ and E_{min} is the energy of the lowest band at $k = 0$. While interpreting the 2D ACAR curves, the enhancement parameters a_l, etc, were determined by a least-squares fit between experiment and theory. Using this phenomenological approach the Geneva group [13, 14] analysed their 2D ACAR data for V, Cr, Fe and Ni, and found that there is de-enhancement of the localized d states and positive enhancement for the s–p states. In the case of paramagnetic Cr Genoud [14] found that the core contribution to $\rho^{2\gamma}(p)$ had to be reduced to 60–70% and the d-electron states were then de-enhanced.

Matsumoto and Wakoh [25] studied the e^+–e^- many-body correlation effects in paramagnetic Cr by using two different phenomenological approaches. The first or the state-dependent approach was similar to that used by the Geneva group [13, 14, 41], and it used separate enhancement factors for the s–p and d electrons. The second approach was called the character-dependent correction, and was applied to the partial (l-dependent) wavefunctions of electrons coupled to the positron. In both approaches the enhancement parameters were determined by obtaining a best fit of the theoretical (using the APW method) 2D ACAR curves to the experiment. These authors observed that in the case of paramagnetic Cr the best fit resulted in a de-enhancement of d-state electrons relative to the s–p states with the core-electron contribution to $\rho^{2\gamma}(p)$ being reduced to about 50%. It was further observed that the character-dependent factors provided better agreement with experiment, thus suggesting that the enhancement correction should be applied in r-space.

Such corrections in r-space have also been developed by Daniuk *et al* [57] and Jarlborg and Singh [58] by using a local-density approach. The method followed

by Daniuk *et al* [57] was based on the Thomas–Fermi approach, and it considered energy-dependent enhancement factors as a function of local electron density, taking into account the local kinetic energy of the electron states. By applying this method for the calculation of 2D ACAR in Zn, it was shown [57] that a better agreement with experiment was obtained by their theory as compared to the IPM theory. In the local-density approach followed by Jarlborg and Singh [58], the enhancement correction was found by solving the Schrödinger equation for the interaction potential between electron and positron. An application of their local enhancement correction to V, Ni and Pd showed an improvement over the IPM results with the enhancement depending on the d-band occupation. However, the local-density approaches of Daniuk *et al* [57] and Jarlborg and Singh [58] did not lead to a perfect agreement between theory and experiment, thus indicating that the e^+–e^- many-body correlation corrections have not been completely understood.

An examination of all these attempts to calculate the e^+–e^- many-body enhancement effects leads to the following conclusions for 3d metals: (i) The enhancement correction is certainly not described by Kahana's formula (1). (ii) The enhancement correction is energy- and l-dependent. (iii) The contribution by the core electrons to $\rho^{2\gamma}(\boldsymbol{p})$ may have to be reduced by a factor α. (iv) In the case of some band-structure calculations, it may be necessary to displace the Fermi energy (E_F) by ΔE ($\sim$ few mRyd) to obtain a better agreement with the experimental Fermi surface [13, 58]. The enhancement corrections are also changed by this procedure. (v) The enhancement effects depend on the position of E_F relative to the centre of d bands [58]. (iv) Various parameters a_l, b_l, c_l, d_l ($l = 0, 1, 2, \ldots$), $\alpha, \Delta E$, etc, have to be determined by obtaining a best fit between theory and experiment.

It is, therefore, clear that, although the e^+–e^- many-body correlation effects play a minor but sensitive role in interpreting the 2D ACAR data for transition metals, it is difficult to calculate them *ab initio*. To achieve success with any phenomenological approach one will require numerical data sets $N(p_y, p_z)$ from a 2D ACAR experiment so that a best fit between theory and experiment is obtained with the help of several parameters involved. In view of the fact that numerical data sets of experimental 2D ACAR for paramagnetic Cr were not available to us, we have not carried out any comparison between the present theory and experiment [11–14] using a phenomenological approach. However, we present the k-space momentum distributions obtained from our results for $\rho^{2\gamma}(\boldsymbol{p})$ in figure 8, and they can be useful to compare similar graphs obtained from the experimental 2D ACAR data by Lock–Crisp–West folding [59]. Figure 8 brings out the familiar features of the Fermi surface topology in paramagnetic Cr. We have also calculated the $B^{2\gamma}(z)$ curves by taking the Fourier transform of $N(p_z)$. These curves along the ⟨100⟩, ⟨110⟩ and ⟨111⟩ directions are not presented here, but they show general shapes similar to the $B(z)$ curves of figure 3, with the differences being attributed to the effects of positron wavefunction [60].

4. Summary and conclusions

Theoretical calculation of $\rho(\boldsymbol{p})$ and $\rho^{2\gamma}(\boldsymbol{p})$ in paramagnetic Cr has been performed using the LCGO method and the same set of electron wavefunctions. Various structures observed in these momentum distributions are discussed in terms of the topology of the Fermi surface. The theoretical $\rho^{2\gamma}(\boldsymbol{p})$ is compared with the experimental results obtained by Kubota *et al* [15] from reconstruction of $\rho^{2\gamma}(\boldsymbol{p})$ from the 2D ACAR data.

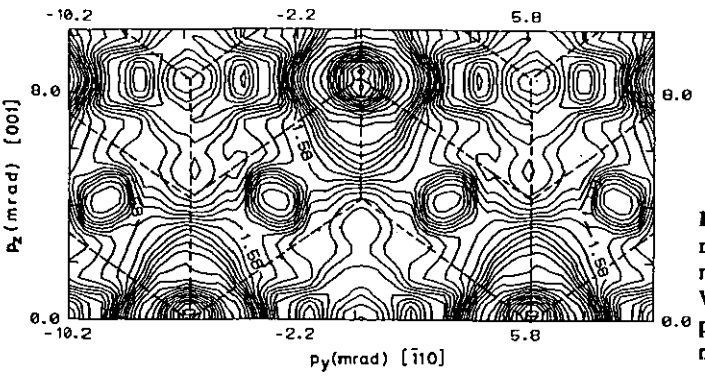

Figure 8. Theoretical *k*-space momentum distributions in paramagnetic Cr obtained by Lock–Crisp–West folding [59] in the (110) plane. The momentum scale is in mrad.

The LCGO method, within the IPM, is found to provide a satisfactory basis to calculate these momentum distributions. The discrepancies observed between the experiment and LCGO theory have been observed previously by the APW theory. These discrepancies arise out of the inadequate description of the Fermi surface, e^-–e^- correlations and e^+–e^- many-body correlations within the IPM and not because of inadequacies of the LCGO theory *vis-à-vis* the APW theory.

Acknowledgments

We are grateful to Professor N Shiotani and Professor S Tanigawa for communicating their results prior to publication. This work was supported by the Department of Science and Technology, Government of India , through grants made to the University of Poona and the Indian Institute of Technology, Kanpur. Similarly, the support given by the Centre for Development of Advanced Computing, Pune, is gratefully acknowledged. Part of this work was carried out by one of us (RMS) at Universität der Bundeswehr, München, and he wishes to thank Alexander von Humboldt Stiftung for a fellowship, and Professor W Triftshäuser for kind hospitality.

References

[1] Overhauser A W 1962 *Phys. Rev.* **128** 1437
[2] Matheiss L F 1965 *Phys. Rev.* **139** A1893
[3] Williams B (ed) 1977 *Compton Scattering* (London: McGraw-Hill)
[4] Cooper M J 1985 *Rep. Prog. Phys.* **48** 415
[5] Berko S 1983 *Positron Solid State Physics* ed W Brandt and A Dupasquier (Amsterdam: North-Holland) p 64
[6] Mijnarends P E 1983 *Positron Solid State Physics* ed W Brandt and A Dupasquier (Amsterdam: North-Holland) p 146; 1979 *Positrons in Solids* ed P Hautojärvi (Berlin: Springer) p 25
[7] Weiss R J 1973 *Phil. Mag.* **27** 1461
[8] Ohara S, Fukamachi T, Hosoya S and Takeda T 1974 *Phys. Soc. Japan* **35** 337
[9] Cardwell D A, Cooper M J and Wakoh S 1989 *J. Phys.: Condens. Matter* **1** 541
[10] Shiotani N, Okada T, Sekizawa H, Wakoh S and Kubo Y 1977 *J. Phys. Soc. Japan* **43** 1229
[11] Bull C R, Alam A, West R N, Shiotani N, Singh A K and Singru R M 1985 *Positron Annihilation* ed P C Jain, R M Singru and K P Gopinathan (Singapore: World Scientific) p 266
[12] Singh A K, Manuel A A and Walker E 1988 *Europhys. Lett.* **6** 67
[13] Manuel A A, Singh A K, Jarlborg T, Genoud P, Hoffman L and Peter M 1988 *Positron Annihilation* ed L Dorikens-Vanpraet, M Dorikens and D Segers (Singapore: World Scientific) p 109

[14] Genoud P 1990 *PhD Thesis* No 2442, University of Geneva (unpublished)
[15] Kubota T, Kondo H, Nakashima H, Murakami Y and Tanigawa S 1991 *Phys. Status Solidi* b **168** 179
[16] Migdal A B 1957 *Sov. Phys.–JETP* **5** 333
[17] Daniel E and Vosko S H 1960 *Phys. Rev.* **120** 2041
[18] Majumdar C K 1965 *Phys. Rev.* **140** A227
[19] Wakoh S, Kubo Y and Yamashita J 1976 *J. Phys. Soc. Japan* **40** 1043
[20] Rath J, Wang C S, Tawil R and Callaway J 1973 *Phys. Rev.* B **8** 5139
[21] Laurent D G, Callaway J, Fry J L and Brener N E 1981 *Phys. Rev.* B **23** 1977
[22] Cardwell D A and Cooper M J 1989 *J. Phys.: Condens. Matter* **1** 9357
[23] Wakoh S and Matsumoto M 1990 *J. Phys.: Condens. Matter* **2** 797
[24] Matsumoto M and Wakoh S 1986 *J. Phys. Soc. Japan* **55** 3948
[25] Matsumoto M and Wakoh S 1987 *J. Phys. Soc. Japan* **56** 3566
[26] Singh A K and Singru R M 1983 *J. Phys. F: Met. Phys.* **13** 2189
[27] Singh A K and Singru R M 1984 *J. Phys. F: Met. Phys.* **14** 1751
[28] Singh A K and Singru R M 1985 *Positron Annihilation* ed P C Jain, R M Singru and K P Gopinathan (Singapore: World Scientific) p 74
[29] Sundararajan V, Kanhere D G and Callaway J 1988 *Phys. Lett.* **133A** 521
Sundararajan V 1988 *PhD Thesis* Anna University, Madras (unpublished)
[30] Callaway J and Wang C S 1977 *Phys. Rev.* B **16** 2095
[31] Wang C S and Callaway J 1978 *Comput. Phys. Commun.* **14** 327
[32] Laurent D G, Wang C S and Callaway J 1978 *Phys. Rev.* B **17** 455
[33] Sundararajan V, Kanhere D G and Singru R M 1992 *Phys. Rev.* B **46** at press
[34] Sundararajan V, Kanhere D G and Singru R M 1991 *J. Phys.: Condens. Matter* **3** 1113
[35] Wang C S and Callaway J 1977 *Phys. Rev.* B **15** 298
[36] Sundararajan V, Asokamani R and Kanhere D G 1988 *Phys. Rev.* B **38** 12653
[37] Jani A R, Brenner N E and Callaway J 1988 *Phys. Rev.* B **38** 9425
[38] Chen H, Brenner N E and Callaway J 1989 *Phys. Rev.* B **40** 1443
[39] Fuster G, Tyler J M, Brenner N E, Callaway J and Bagayoko D 1990 *Phys. Rev.* B **42** 7322
[40] Sundararajan V and Kanhere D G 1990 *Pramana J. Phys.* **34** 33
[41] Singh A K, Manuel A A, Jarlborg T, Mathys Y, Walker E and Peter M 1986 *Helv. Phys. Acta* **59** 410
[42] Kanhere D G 1992 private communication
[43] Barbiellini B and Jarlborg T 1989 *J. Phys.: Condens. Matter* **1** 8865
[44] von Barth U and Hedin L 1972 *J. Phys. C: Solid State Phys.* **5** 1629
[45] Rajagopal A K, Singhal S P and Kimball J (unpublished) as quoted by Rajagopal A K 1979 *Advances in Chemistry and Physics* vol 41, ed G I Prigogine and S A Rice (New York: Wiley) p 59
[46] Moruzzi V L, Janak J F and Williams A R 1978 *Calculated Electronic Properties of Metals* (Oxford: Pergamon)
[47] Sakai N 1992 *Mater. Sci. Forum* **105–110** 431
[48] Biggs F, Mendelsohn L B and Mann J B 1975 *At. Data Nucl. Data Tables* **16** 201
[49] Schülke W 1977 *Phys. Status Solidi* b **82** 229
[50] Hansen N K, Pattison P and Schneider J R 1979 *Z. Phys.* B **35** 215
[51] Harthoorn R and Mijnarends P E 1978 *J. Phys. F: Met. Phys.* **8** 1147
[52] Pecora L M 1989 *J. Phys.: Condens. Matter* **1** SA1; 1987 *IEEE Trans. Nucl. Sci.* NS-34 642
[53] Pecora L M, Ehrlich A C, Manuel A, Singh A K, Peter M and Singru R M 1988 *Phys. Rev.* B **37** 6772
[54] Kahana S 1963 *Phys. Rev.* **129** 1622
Carbotte J P and Kahana S 1965 *Phys. Rev.* **139** A213
[55] Sob M 1978 *Proc. 8th Gaussig Conf. (Dresden, 1978)* ed P Ziesche (unpublished); 1982 *J. Phys. F: Met. Phys.* **12** 571
[56] Mijnarends P E and Singru R M 1979 *Phys. Rev.* B **19** 6038
[57] Daniuk S, Kontrym-Sznajd G, Mayers J, Rubaszek A, Stachowiak H, Walters P A and West R N 1987 *J. Phys. F: Met. Phys.* **17** 1365
[58] Jarlborg T and Singh A K 1987 *Phys. Rev.* B **36** 4660
[59] Lock D G, Crisp V H C and West R N 1973 *J. Phys. F: Met. Phys.* **3** 561
[60] Singh A K, Manuel A A, Singru R M and Peter M 1985 *Helv. Phys. Acta* **58** 640